Proceedings of the 37th International & 4th National Conference on Fluid Mechanics and Fluid Power

FMFP2010

December 16-18, 2010, IIT Madras, Chennai, India

FMFP2010 CF - 09

NUMERICAL SIMULATION OF VISCOUS FLOW OVER A SQUARE CYLINDER ON GRADED CARTESIAN MESHES USING MULTIGRID METHOD

D. Santhosh Kumar
School of Mechanical & Building Sciences
Vellore Institute of Technology
Vellore - 632014, India
E-mail: santhoshkumar.d@vit.ac.in

Anoop K Dass
Department of Mechanical Engineering
Indian Institute of Technology Guwahati
Guwahati - 781039, India
E-mail: anoop@iitg.ernet.in

Anupam Dewan
Department of Applied Mechanics,
Indian Institute of Technology Delhi,
New Delhi - 110016, India
E-mail: adewan@am.iitd.ac.in

ABSTRACT

This paper deals with the computation of laminar viscous flow past a square prism confined in a channel using multigrid method on graded Cartesian meshes. As the finite difference method is used to discretize the governing equations on nonuniform staggered grids, a transformation of the governing equations from the physical space to the computational space is performed. In the computations of transient viscous flows the pressure-Poisson equation has to be solved accurately at every time-step and it is imperative that this computation is carried out with good time-wise efficiency. Therefore multigrid method is employed to accelerate the convergence of the Poisson equation. To obtain second-order time accuracy a fractional-step method is employed. The convective terms are discretized using a third-order accurate upwind scheme and the viscous terms are centrally differenced to fourth-order accuracy. The code is validated by computing the well known lid-driven cavity flow problem. After having thus gained confidence in the code it is then applied to compute the flow past a square prism. Accurate results in the shape of instantaneous streamlines and vorticity contours are plotted for various Reynolds numbers. Periodicity of the flow is established through phase plots, power spectrum analysis and temporal plots of lift and drag coefficients.

Several flow parameters are computed and compared with established results to demonstrate that the multigrid strategy adopted here affords an efficient and accurate procedure for computing this interesting flow configuration rich in fluid mechanical features.

Keywords: Fractional-step method, square cylinder, multigrid method, nonuinform grid, grid transformation.

INTRODUCTION

The unsteady incompressible flows occur frequently in problems of academic interest and engineering applications and one approach adopted for the solution of the unsteady, incompressible Navier-Stokes equations is the fractional-step method (Kim and Moin, 1985). In this approach the time integration of the Navier-Stokes equations is carried out by means of the fractional-step procedure, whereby at each time step an incomplete form of the momentum equations is integrated to yield an approximate velocity field, which will in general not be divergence-free. Subsequently a correction is applied to the approximate velocity field to produce a divergence-free velocity field. Integration then proceeds to the next time-step. The correction takes the form of the gradient of a scalar, with the scalar field obtained by solving a Poisson equation with the divergence of the approximate velocity as the right hand side. The scalar itself is either the pressure or a pressure correction, depending on the exact form of the fractional-step scheme being used. In the present work the scalar is the pressure instead of pressure correction. Such schemes are called projection methods as the correction to the velocity is accomplished via an orthogonal projection onto the divergence-free field.

Finite difference method is frequently used in computational fluid dynamics. The method essentially involves setting up a suitable grid in the problem domain, discretizing the governing equations with respect to the grid and solving them numerically. The common practice is to use a uniform grid, though it may not be the most appropriate one for an efficient computation. An accurate spatial resolution of the solution requires that grid points are clustered in the regions of large gradients. Hence nonuniform grids are used for many flow configurations. Finite difference formulations cannot be easily applied on nonuniform grids. The usual approach adopted is to map the physical space with a nonuniform grid on to a computational space with uniform grid where a transformed set of equations is first solved before mapping this solution back on the physical space for interpretation. The disadvantage of this approach is that, there is an increase in the number of terms to be discretized in the transformed governing equations giving rise to added computations (Kalita *et al*., 2004). Many times, however, advantages of using a nonuniform grid outweigh the disadvantages mentioned above. By use of nonuniform grids it is possible to cluster grid lines in the regions of sharp gradients and use a relatively coarser grid in the regions involving small gradients, thus obtaining a better spatial scale resolution with a smaller overall grid size. It has already been mentioned that the transformed governing equations contain a larger number of terms than the original equations, which may result in some increase in the computational cost. Particularly, the pressure-Poisson equation that requires very accurate solution at every time step and consumes more than eighty percent of the total computational time needs special attention and an efficient algorithm for its numerical solution is highly desirable. Multigrid, which is arguably the best general convergence acceleration technique (Tannelhill *et al*., 1997), has been found to work efficiently especially when the grid size is large. This is the reason why multigrid technique is used in the present paper to compute the pressure-Poisson equation. In this paper the performance of the multigrid method in the numerical solution of the pressure-Poisson equation on graded Cartesian meshes is also examined in some details. Expectedly multigrid accelerates the convergence of the Gauss-Seidel iterations significantly, which in turn brings about a

substantial reduction of cost in the overall transient flow computation.

In the present work a finite-difference discretization of the governing equations is carried out on a staggered grid (Patankar and Spalding, 1972). As the time accuracy of the fractional-step method used in this work is also of second order, the transient results produced here have the potential of being very accurate. This aspect of the code is examined by first applying it to compute the transient flow in a single-sided lid-driven cavity and then the time-marching steady flow in the same configuration. Close agreement with validated results proves the accuracy of the present computation. The code is then used to solve flow past a square prism confined in a channel to study the vortex shedding and, lift and drag behaviour. Use of high-precision arithmetic to offset accumulation of round-off errors in the transient computations lends added credibility to the results. Thus, development of an accurate and efficient computational tool for computing incompressible transient-viscous flows using multigrid method may be considered the main achievement of this work.

GOVERNING EQUATIONS

The unsteady, 2D, incompressible N-S equations in the traditional primitive variable formulation in the non-dimensional form can be written as

$$\frac{\partial u}{\partial x}+\frac{\partial v}{\partial y}=0 \tag{1}$$

$$\frac{\partial u}{\partial t}+\frac{\partial (u^2)}{\partial x}+\frac{\partial (uv)}{\partial y}=-\frac{\partial p}{\partial x}+\frac{1}{Re}\left(\frac{\partial^2 u}{\partial x^2}+\frac{\partial^2 u}{\partial y^2}\right) \tag{2}$$

$$\frac{\partial v}{\partial t}+\frac{\partial (uv)}{\partial x}+\frac{\partial (v^2)}{\partial y}=-\frac{\partial p}{\partial y}+\frac{1}{Re}\left(\frac{\partial^2 v}{\partial x^2}+\frac{\partial^2 v}{\partial y^2}\right) \tag{3}$$

Here u and v denote the velocities along x- and y-directions, t the time and p the pressure, respectively. In view of Eq. (1) the solenoidality of the velocity field must be ensured at every instant in a transient computation. The solution of Eqs. (1) - (3) confronts difficulties like the lack of an independent equation for the pressure and non-existence of a dominant variable in the continuity equation. Therefore, pressure is treated explicitly by solving a pressure-Poisson equation. We will see later the form of the pressure-Poisson equation in the context of the fractional-step method. The solution of governing equations (1) - (3) on graded Cartesian meshes using the finite difference method makes it is necessary to transform the equations from the physical to the computational planes. The details of the transformation are given in Santhosh *et al*. (2010). Using the transformation, the governing equations in the computational plane corresponding to the equations (1-3) in the physical plane now become

$$\xi_x \frac{\partial u}{\partial \xi}+\eta_y \frac{\partial v}{\partial \eta}=0 \tag{4}$$

$$\frac{\partial u}{\partial t}+(u\xi_x)\frac{\partial u}{\partial \xi}+(v\eta_y)\frac{\partial u}{\partial \eta}=-\xi_x \frac{\partial p}{\partial \xi}+\frac{1}{Re}\left(\xi_{xx}\frac{\partial u}{\partial \xi}+\xi_x^2\frac{\partial^2 u}{\partial \xi^2}\right)+\frac{1}{Re}\left(\eta_{yy}\frac{\partial u}{\partial \eta}+\eta_y^2\frac{\partial^2 u}{\partial \eta^2}\right) \tag{5}$$

$$\frac{\partial v}{\partial t}+(u\xi_x)\frac{\partial v}{\partial \xi}+(v\eta_y)\frac{\partial v}{\partial \eta}=-\eta_y \frac{\partial p}{\partial \eta}+\frac{1}{Re}\left(\xi_{xx}\frac{\partial v}{\partial \xi}+\xi_x^2\frac{\partial^2 v}{\partial \xi^2}\right)+\frac{1}{Re}\left(\eta_{yy}\frac{\partial v}{\partial \eta}+\eta_y^2\frac{\partial^2 v}{\partial \eta^2}\right) \tag{6}$$

FRACTIONAL-STEP PROCEDURE

The four-step fractional-step method (Kim and Moin, 1985) employed in the present paper is now described in some detail. In the first step the momentum equation (7) is solved for an auxiliary velocity field $\hat{u}_i$ using the pressure from the previous time step; the convective terms and viscous terms are solved explicitly using the second-order Adams-Bashforth method.

$$\frac{\hat{u}_i-u_i^n}{\Delta t}=-\frac{\partial p^n}{\partial x_i}+\frac{1}{2}\left[3H\left(u_i^n\right)-H\left(u_i^{n-1}\right)\right] \tag{7}$$

where H is an operator representing the discretized convective and diffusive terms. In the second step Eq. (8) is solved to advance the auxiliary velocity field which is of course not divergence-free.

$$\frac{u_i^*-\hat{u}_i}{\Delta t}=\frac{\partial p^n}{\partial x_i} \tag{8}$$

In the third step, the incompressibility condition is enforced by solving the pressure Poisson Eq. (9), which is obtained by taking the divergence of Eq. (10) satisfying continuity for the next time step.

$$\frac{\partial}{\partial x_i}\frac{\partial p^{n+1}}{\partial x_i} = \frac{1}{\Delta t}\frac{\partial u_i^*}{\partial x_i} \quad (9)$$

Finally in the fourth step the velocity which satisfies the incompressibility condition is obtained by using the following correction step:

$$\frac{\left(u_i^{n+1} - u_i^*\right)}{\Delta t} = -\frac{\partial p^{n+1}}{\partial x_i} \quad (10)$$

The Poisson equation in the physical plane is given by Eq. (9) in the tensor form. This equation in the transformed plane, which is solved using the multigrid method at each time step to satisfy the divergence-free condition, may be written in the expanded form as

$$\xi_{xx}\frac{\partial p}{\partial \xi} + \xi_x^2\frac{\partial^2 p}{\partial \xi^2} + \eta_{yy}\frac{\partial p}{\partial \eta} + \eta_y^2\frac{\partial^2 p}{\partial \eta^2} = \sigma \quad (11)$$

where, σ is the source term that has the form

$$\frac{1}{\Delta t}\left(\xi_x\frac{\partial u^*}{\partial \xi} + \eta_y\frac{\partial v^*}{\partial \eta}\right)$$

NUMERICAL METHOD

The governing equations are discretized in space, using a finite difference formulation on a staggered, Cartesian grid, where velocities and pressure are calculated at different locations. The main advantage of the staggered grid arrangement is the strong coupling between pressure and velocities without requiring special interpolation techniques. This helps avoid convergence problems and oscillations in pressure fields. Another advantage of using staggered grid for incompressible flows is that the pressure boundary conditions are not required when the momentum equations are evaluated. For the pressure-Poisson equation the pressure gradient normal to the walls is assumed zero, i.e.,

$$\frac{\partial p}{\partial x_i} = 0 \quad (12)$$

The convective terms of the momentum equations are approximated with Kuwahara's third-order upwind scheme (Kawamura and Kuwahara, 1984) (Eq. 13) and viscous terms are discretized with a fourth-order central-difference scheme (Eq. 14) as given below:

$$\left(u\frac{\partial u}{\partial \xi}\right)_{i,j} = u_{i,j}\left(u_{i-2,j} - 8u_{i-1}, j + 8u_{i+1,j} - u_{i+2,j}\right)/12\Delta\xi + \left|u_{i,j}\right|\left(u_{i-2,j} - 4u_{i-1,j} + 6u_{i,j} - 4u_{i+1,j} + u_{i+2,j}\right)/4\Delta\xi \quad (13)$$

$$\left(\frac{\partial^2 u}{\partial \xi^2}\right)_{i,j} = \left(-u_{i-2,j} + 16u_{i-1,j} - 30u_{i,j} + 16u_{i+1,j} - u_{i+2,j}\right)/\left(12(\Delta\xi)^2\right) \quad (14)$$

COMPUTATIONS RESULTS AND DISCUSSIONS

The code developed is second-order accurate in time, third-order accurate in the spatial discretization of the convective terms and fourth-order accurate in the spatial discretization of the viscous terms. In order to evaluate the performance of the code in regard to timewise efficiency and accuracy, it is first applied to single-sided lid-driven cavity flow which asymptotically reaches steady state if the solution is advanced sufficiently long in time.

Multigrid Solutions of Pressure-Poisson Equation

In the present study a 4-level V-cycle multigrid shown in Fig. 1 has been used in all the computations to solve the pressure-Poisson equation and the number of sweeps used in various grid-levels is given inside the corresponding circles. For a 2-level scheme on a 129 × 129 grid at *Re* = 3200, performance is seen to improve by increasing the number of sweeps in the coarser grid. When the number of sweeps increases from 7 to 60, the number of equivalent fine grid sweeps required for the convergence ultimately reduce from 927 to 321, which represents a reduction of computational effort to nearly one-third for the 2-level scheme. For *Re* = 3200 on a 129×129 grid, it is observed that using four or five level of grids is good enough as further increase of levels produce no time-wise gain. Specifically, it was observed that 3736, 321, 164, 36, 29, 29 and 29 work units (WU) (equivalent fine-grid sweeps) were required when using 1−, 2−, 3−, 4−, 5−, 6− and 7-levels respectively [Fig. 2(a)]. To gain an insight into the convergence behaviour after around 100 time steps, at *t* = 0.1 a plot between the pressure error and

number of iterations required to solve the pressure-Poisson equation is shown in Fig. 2(b). Before examining overall quantitative performance data, it is instructive to consider the convergence histories in

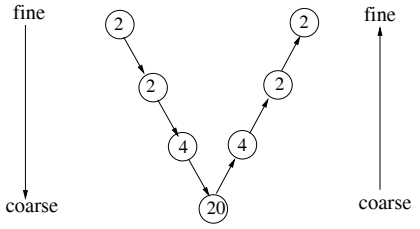
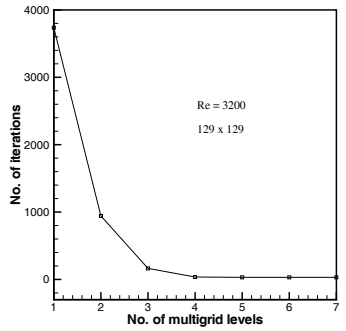
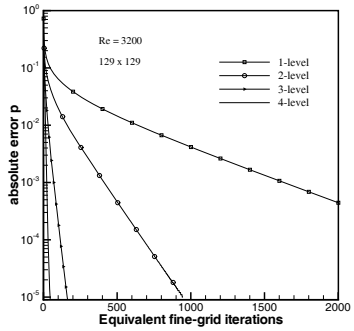


Fig. 1 V-cycle multigrid showing iterations at various levels.



(a) Effect of multigrid levels



(b) Pressure error history.

Fig. 2 Convergence of multigrid on a 129 × 129 grid for Re = 3200 at t = 0.1.

Fig. 2(b) obtained with the single grid and with sequences of 2-, 3- and 4-levels. Expectedly the convergence curves relating to multigrid are considerably steeper than those relating to the single grid. The ratio of the computational effort in work units for the single grid to that for the multigrid may be termed as speed-up. As the convergence limit of error is lowered speed-up is seen to increase. This is because on a single grid error-reduction rate becomes smaller and smaller as the iteration progresses whereas multigrid maintains more or less the same error-reduction rate throughout. The performance of the multigrid with the optimum number of levels is truly amazing. The number of sweeps is seen to be nearly independent of the number of grid points used. Only 29 sweeps were required for the finest grid compared to 3736 for the conventional Gauss-Seidel method. This is a reduction in effort by a factor of 128.

Grid- and Time-Step-Independence Study

Fig. 3 shows the horizontal velocity along the vertical centreline of the cavity at instant t = 20.0 captured with three different time steps Δt = 0.001, 0.0005 and 0.0001 for Re = 3200. These profiles plotted for a 129 × 129 grid show no discernable differences, proving the time-accuracy of the present computations together with the fact that the transient results are also physically meaningful. Therefore, a time step of 0.001 has been used for all subsequent computations. Fig. 4 presents a comparison of the steady-state horizontal velocities on the vertical centreline of the square cavity with those obtained by Botella and Peyrett (1998). The presents results agree well with those reported in the literature.

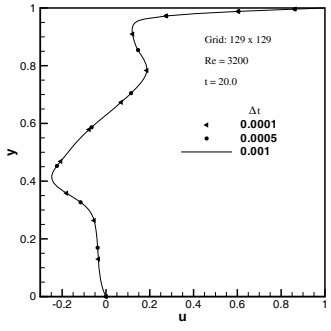


Fig. 3 Time-step-independence study for u-velocity along vertical centerline.

Multigrid Performance

Table 1 gives the CPU times of multigrid and single grid computations to reach the symptotic steady state and the time-wise speed-up achieved by multigrid for various Reynolds numbers on a grid of

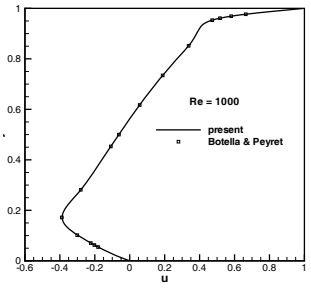


Fig. 4 Comparison of steady-state centreline *u*-velocity for lid-driven cavity flow.

size 129 × 129. For the same fall of residual, time-gain by multigrid is impressive. The time-wise speed-up achieved by multigrid at 'steady state' is nine or slightly less. It is also observed that work units required to reach the steady state increase as *Re* increases for both single-grid and multigrid. This can be attributed to the fact that high Reynolds number flows contain multiplicity of scales, which introduce high frequency errors into the computational process. The time-wise speed-up achieved by multigrid is also seen to decrease as *Re* increases.

Table 1: Performance of multigrid for a 129 × 129 grid on a nonuniform grid at various Reynolds numbers

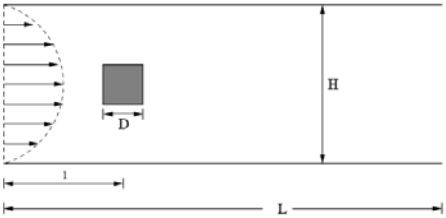
Re	CPU time (minutes)		Speed-up
	Single-grid	MG 4-level	
1000	1557	161	9.8
3200	3872	412	9.4
5000	5353	645	8.3
7500	7163	885	8.1

FLOW PAST A SQUARE PRISM

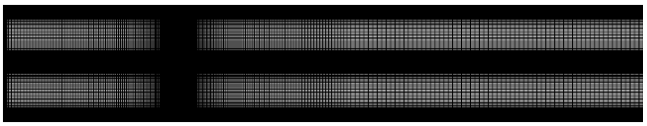
The viscous flow past a bluff body and the resulting separated region behind it, has been the focus of numerous experimental and numerical investigations. The presence of wall confinement is one of the most common examples in practical flow situations (e.g., the flow situation in wind tunnels, flow around tall buildings and bridges, etc.) and therefore the study of effect of wall confinement on flow field characteristics is of crucial importance. Studies on problems of wake development and vortex shedding behind a two-dimensional rectangular prism in confined and un-confined flows have been investigated numerically and experimentally by Davis *et al*. (1984). From the literature, it is observed that when bounding walls are present in the flow, the behaviour of vortex shedding behind the body is affected significantly. It should be stated clearly that the objective of the present work is to demonstrate the reliability of the present code to capture the vortex shedding. The domain of the flow is multiply connected and the nature of the flow itself is very complex. At sufficiently high Reynolds numbers, owing to the wake instability mechanisms the vortical region downstream of the body breaks into the phenomenon of vortex shedding characterized by an unsteady periodic flow situation in which the separated vortices are shed alternately from the upper and lower sides of the body. The unsteady behaviour of the flow that evolves with time for Reynolds numbers beyond a critical value makes this problem quite challenging and interesting. Thus, simulation of this flow configuration is a good test case to check the robustness and reliability of the present code. The flow configuration is similar to those of (Breuer *et al*., 2000) as shown in Fig. 5(a). It has a prism with square cross-section with width D that is mounted centrally inside a plane channel of height H with blockage ratio $B = D/H = 1/8$. The channel length L is fixed at $L/D = 50$ to reduce the influence of inflow and outflow boundary

conditions. An inflow length of $l = L/4$ has been chosen. At the inlet, a parabolic velocity profile is introduced while at the outlet, convective boundary conditions given by

$$\frac{\partial \phi}{\partial t} + u_{conv} \frac{\partial \phi}{\partial t} = 0 \qquad (15)$$



(a)



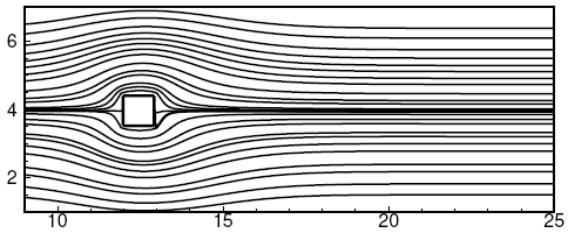
(b)

Fig. 5 (a) Configuration of flow past a square prism
(b) Grid arrangement

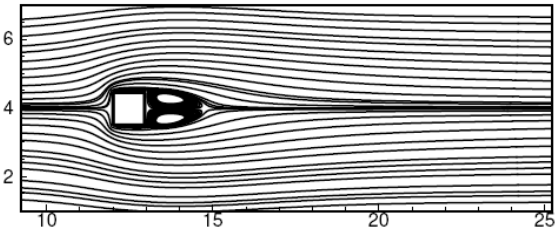
has been used with φ standing for u and v, while u_{conv} is set equal to the maximum u-velocity at the inlet. This condition ensures that vortices can approach and pass the outflow boundary without significant disturbances or reflections into the inner domain. The no-slip boundary conditions are applied on the surface of the square prism and on both the upper and lower walls.

The present study uses non-uniform Cartesian grids. This has the advantage that grid points can be clustered in regions of large gradients, i.e., in the vicinity of the square prism and coarser grids can be used in regions with small gradients [see Fig. 5(b)]. A 1024 × 128 grid is used in the present study. This flow configuration has been solved for the Reynolds numbers 1, 30 and 100 where *Re* is based on the prism side and the maximum flow velocity u_{max} of the parabolic inflow profile. Fig. 6 shows the computed streamlines at three different Reynolds numbers *Re* = 1, 30 and 100 each characterising a different flow regime. At low *Re* = 1, the creeping steady flow past the square prism persists without separation [Fig. 6(a). Relative magnitude of viscous forces decreases with an increasing *Re* until at a certain value a separation of the laminar boundary layer occurs. As *Re* increases separation at the trailing edges of the sharp-edged body can be observed. At *Re* = 30, the wake comprises a steady recirculation region of two symmetrically placed vortices on each side of the channel centreline as shown in Fig. 6(b). Figure 6(c) shows a typical instantaneous streamline pattern for unsteady flow at *Re* = 100. The corresponding vorticity contours for *Re* = 1, 30 and 100 are depicted in Fig. 7(a-c). Literature states that initially the size of the recirculation region increases with an increase in *Re* and when a critical Reynolds number is exceeded, the well known von Karman vortex street with periodic vortex shedding from the prism can be detected in the wake. Based on experimental investigations, Okajima (1982) found periodic vortex motion at Re ≈ 70 leading to an upper limit of $Re_{\text{crit}} \leq 70$. A smaller value ($Re_{\text{crit}} = 54$) was determined by Kelkar and Patankar (1992) based on a stability analysis of the edges of the prism. Present computations at *Re* = 100 [Fig. 7(c)] show that the free shear layers roll up and form eddies. This phenomenon is popularly known as the von Karman vortex shedding and the corresponding streamline pattern is shown in Fig. 6(c). The temporal evolution of the streamline patterns over one complete period is shown in Fig. 8. The streamlines are wavy and sinuous on the leeward side of the square prism. However, the upstream depicts a potential-flow-like pattern. Two eddies are shed within each period from the aft of the square prism. These eddies are formed behind the prism and are washed away into the wake region. The temporal evolution of the vorticity contours over one complete vortex shedding cycle is depicted in Fig. 9. The vorticity contours reveal several additional features which could not be directly perceived from the streamlines. The staggered nature of the Karman shedding is clearly seen from these plots. The eddies are alternately of positive and

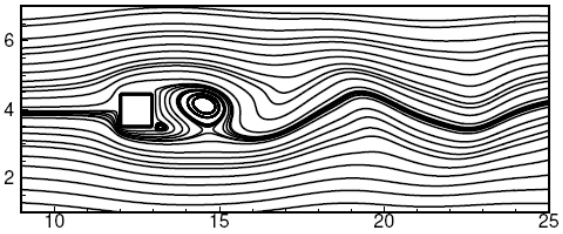
negative vorticity. This is manifested in the form of crests and troughs in the sinuous shape of the streamlines.



(a) *Re* = 1

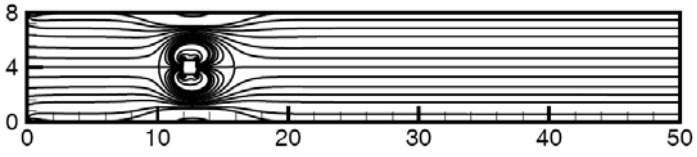


(b) *Re* = 30

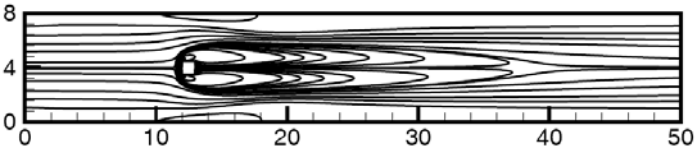


(c) *Re* = 100

Fig. 6 Streamline patterns for flow past a square prism at various Reynolds numbers.



(a) *Re* = 1



(b) *Re* = 30



(c) *Re* = 100

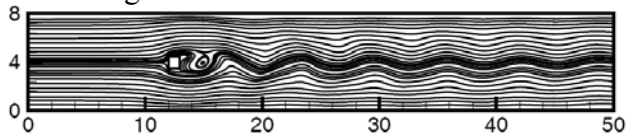
Fig. 7 Vorticity contours for flow past a square prism at various Reynolds numbers.

The two most important characteristic quantities of flow around a prism are the drag coefficient (C_D) and the lift coefficient (C_L). The coefficients C_D and C_L are defined as $F_D / \frac{1}{2}\rho u_{\max}^2 D$ and $F_L / \frac{1}{2}\rho u_{\max}^2 D$, where F_D and F_L denote the drag and lift force on the square prism, respectively. The drag force (F_D) is calculated by the expression $\sum_1 p\,\delta y - \sum_2 p\,\delta y$, where the suffixes 1 and 2 denotes the forward and rear sides of the prism. The lift force (F_L) is calculated by the expression $\sum_3 p\,\delta x - \sum_4 p\,\delta x$, where the suffixes 3 and 4 denotes the top and bottom sides of the prism. Fig. 10(a) presents the time history of the drag coefficient (C_D) and lift coefficient (C_L) after the flow has attained periodicity. The periodic eddy shedding is reflected in the fluctuating drag and lift coefficient history. It is reported that the C_D of the square prism has a higher value than the C_D of a circular cylinder. Fig. 10(a) shows that for each time period C_D has two crests and two troughs of unequal amplitudes, which are a consequence of the periodic vortex shedding from the top and bottom surfaces. The same figure shows that C_L for each time period has just one trough and one crest; this is because C_L is not influenced by the pressure distribution on the right face, which is strongly influenced by the vortex shedding at the top and bottom surfaces. The value of the lift force fluctuation is directly connected to the formation and shedding of the eddy and, therefore, its value varies between a positive maximum and a negative maximum of equal magnitude.

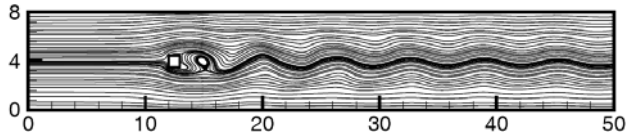
A power spectrum plotted in Fig. 10(b) for C_L using the Fourier analysis confirms that the solution is periodic with one dominant harmonic and its corresponding frequency is 0.137. After the flow reaches a stable periodic state, a phase diagram [Fig. 10(c)] is drawn between u and v at the monitoring point (53/4, 14/4). These plots indicate a perfect periodic pattern for the solutions obtained. Another important quantity considered in the present analysis is the Strouhal number (St), computed from the prism width D, the measured frequency of the vortex shedding f and the maximum velocity u_{max} at the inflow plane through the relation

$$St = \frac{fD}{u_{\max}} \qquad (16)$$

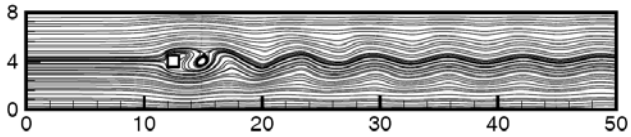
where f, the frequency of vortex shedding, is determined by a spectral analysis of the time series of the lift coefficient C_L [Fig. 10(b))]. The mean drag coefficient (C_{Dmean}) is calculated by time-averaging C_D for integral number of cycles using the Simpson's one-third rule. The computed C_{Dmean} and Strouhal number are compared with earlier results reported in the literature and are shown in Table 2. The present results are in good agreement with earlier investigations.



(a) $t = t_0$

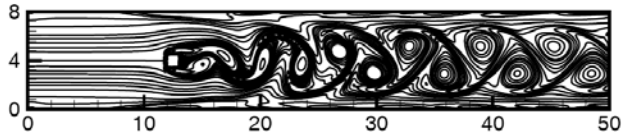


(b) $t = t_0 + T/2$

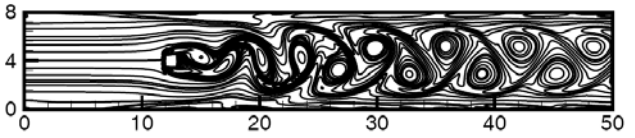


(c) $t = t_0 + T$

Fig. 8 Temporal evolution of streamline patterns over one period at Re = 100.



(a) $t = t_0$

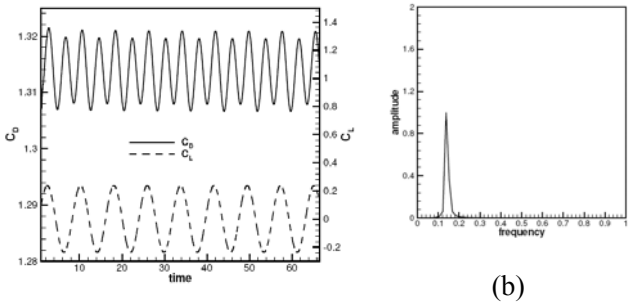


(b) $t = t_0 + T/2$

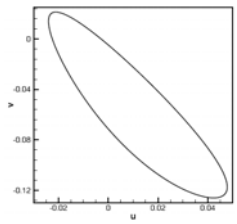


(c) $t = t_0 + T$

Fig. 9 Temporal evolution of vorticity contours over one complete vortex shedding cycle.



(a) (b)



(c)

Fig. 10 (a) Variation of drag and lift coefficients (b) Power spectrum of C_L (c) Phase diagram

Table 2: Comparison of C_{Dmean} and Strouhal number

	Breuer *et al.* (2000)	De and Dalal (2007)	Present
C_{Dmean}	1.37	1.31	1.318
Strouhal number	0.139	0.142	0.137

CONCLUSIONS

The main aim of the present work is the development of a 2D transient Navier-Stokes solver and test its capability in complex situations. In the efficiency front, to achieve grid economy graded Cartesian meshes coupled with grid-transformation are used and to enhance the time-wise efficiency, multigrid method is used to solve the cumbersome pressure-Poisson equation that needs to be solved at every time step in a transient solver. After having first validated the code by computing the classical 2D lid-driven cavity flow, the flow over a square prism is computed. Care has been taken to produce results independent of the space-grid and time step. The problem of flow over a square prism confined in a channel has many interesting features that include the famous von Karman vortex street. The present work demonstrates that these flow features can be efficiently captured using the multigrid method. The demonstration of periodicity through the power spectrum analysis, phase plot and, the C_D and C_L *vs* time plot conclusively shows the periodic nature of the flow. The C_D *vs* time plot is particularly interesting in that in a period there are two troughs and two crests of unequal magnitudes.

REFERENCES

1. Botella, B, Peyret, R., 1998. Benchmark spectral results on the lid-driven cavity flow. Computers and Fluids 27:421–433.
2. Breuer, M, Bernsdorf, J, Zeiser, T, and Durst, F., 2000. Accurate computations of the laminar flow past a square cylinder based on two different methods: lattice-Boltzmann and finite volume, International Journal of Heat and Fluid Flow, 21:186–196.
3. De, A.K.,and Dalal, A, 2007. Numerical study of laminar forced convection fluid flow and heat transfer from a triangular cylinder placed in a channel, Transactions of the ASME, 129:646–656.
4. Davis, R.W., Moore, E.F., Purtell, L.P., 1984. A numerical-experimental study of confined flow around rectangular cylinders, Physics of Fluids, 27:46–59.
5. Kalita, J.C., Dass, A.K., Dalal, D.C., 2004. A transformation-free HOC scheme for steady convectiondiffusion on nonuniform grids, International Journal of Numerical Methods in Fluids 44:33–53.
6. Kawamura, T, Kuwahara, K, 1984. Computation of high Reynolds number flow around a circular cylinder with surface roughness. AIAA Journal 84:0340.
7. Kim J, Moin P, 1985. Application of a fractional-step method to incompressible Navier-Stokes equation, Journal of Computational Physics 59:308–323.
8. Kelkar, K.M., Patankar, S.V., 1992. Numerical prediction of vortex shedding behind a square cylinder, International Journal for Numerical Methods in Fluids, 14:327–341.
9. Okajima, A, 1982. Strouhal numbers of rectangular cylinders. Journal of Fluid Mechanics, 123:379–398.
10. Patankar, S.,V., Spalding, D, 1972. A calculation procedure for heat, mass and momentum transfer in three-dimensional parabolic flows, International Journal of Heat and Mass Transfer 15:1787–1806.
11. Santhosh Kumar, D, Dass, A. K., Dewan, A, 2010. Multigrid Accelerated Computation of 2D Time-Dependent Incompressible Viscous Flows, Engineering Applications of Computational Fluid Mechanics, 4 :71-90.
12. Tannnelhill, J.C., Anderson, D.A., Pletcher, R.H., 1984. Computational fluid mechanics and heat transfer, 2nd Edition. New York: Hemisphere Publishing Corporation.